Modulus–Pressure Equation for Confined Fluids

Gennady Y. Gor,[1,*] Daniel W. Siderius,[2] Vincent K. Shen,[2] and Noam Bernstein[3]

[1] *NRC Research Associate, Resident at Center for Materials Physics and Technology, Naval Research Laboratory, Washington, DC 20375, USA*

[2] *Chemical Sciences Division, National Institute of Standards and Technology, Gaithersburg, MD 20899, USA*

[3] *Center for Materials Physics and Technology, Naval Research Laboratory, Washington, DC 20375, USA*

(Dated: February 9, 2017)

Abstract

Ultrasonic experiments allow one to measure the elastic modulus of bulk solid or fluid samples. Recently such experiments have been carried out on fluid-saturated nanoporous glass to probe the modulus of a confined fluid. In our previous work [J. Chem. Phys., (2015) **143**, 194506], using Monte Carlo simulations we showed that the elastic modulus K of a fluid confined in a mesopore is a function of the pore size. Here we focus on modulus-pressure dependence $K(P)$, which is linear for bulk materials, a relation known as the Tait-Murnaghan equation. Using transition-matrix Monte Carlo simulations we calculated the elastic modulus of bulk argon as a function of pressure and argon confined in silica mesopores as a function of Laplace pressure. Our calculations show that while the elastic modulus is strongly affected by confinement and temperature, the slope of the modulus versus pressure is not. Moreover, the calculated slope is in a good agreement with the reference data for bulk argon and experimental data for confined argon derived from ultrasonic experiments. We propose to use the value of the slope of $K(P)$ to estimate the elastic moduli of an unknown porous medium.

Keywords: Nanopore, Confined Fluids, Tait-Murnaghan equation, Bulk modulus, Ultrasonics

* Currently at: Otto H. York Department of Chemical, Biological, and Pharmaceutical Engineering, New Jersey Institute of Technology, University Heights, Newark, NJ 07102, USA.

URL: `http://porousmaterials.net`. Corresponding author, e-mail: gor@njit.edu

I. INTRODUCTION

When fluids are confined to nanometer-scale pores, their thermodynamic and dynamic properties can significantly differ from those of bulk fluids [1]. Simple examples of these changes are shifts of the temperatures and pressures at which phase transitions occur [2–4], and the development of extremely high pressures [5–7], etc. Experimental studies of properties of confined fluids often presents a challenge, and in recent years much effort has been spent employing various techniques, primarily X-ray [5] and neutron scattering [8, 9]. Interestingly, very short wavelength tools are not the only ones able to shed light on the nano-confined fluid properties, but also long wavelength tools, such as ultrasonic acoustic waves.

In 1982 Murphy carried out the first ultrasonic study on a fluid-saturated Vycor glass, which was focused mainly on sound attenuation [10]. This work introduced the use of ultrasound for studies of properties of matter in nanometer confinement of Vycor pores, which has been employed in numerous works since then. Beamish and co-workers used it to study the properties of liquid helium [11–13] and also proposed ultrasonic experiments for probing the surface area of nanoporous materials [14]. Later ultrasonic experiments became widely used for studying phase transitions in confinement, both liquid-vapor [15–18] and solid-liquid [19–28]. Among these works, it is worth pointing out the paper of Page et al. [16], which first showed that when the pores are completely filled with a liquid-like capillary condensate, the modulus of the fluid (n-hexane) was not constant, but a monotonic function of the gas pressure p (lower pressure corresponds to lower modulus). Moreover, they explained this regularity by the negative Laplace pressures due to menisci at the liquid-vapor interfaces below saturation. More recently Schappert and Pelster carried out a similar experiment, but using argon at cryogenic temperatures [18], and their results were consistent with the results of Page et al.

These studies motivated us to perform calculations of the elastic modulus of confined argon using molecular models. First we derived the elastic modulus from the *average* density of confined argon, predicted by classical density functional theory (cDFT) [29]. Our calculations reproduced the experimentally observed linear relation between the modulus and the solvation pressure (also referred to as the adsorption stress), and the slope in this relation was close to the slope reported in ultrasonic experiments [18]. Those calculations,

however, required use of macroscopic Gibbs-Duhem equation, whose validity is not obvious for a confined system. Therefore in our following work [30] we performed calculations of the elastic modulus of confined argon based on fluctuations of the number of particles in grand canonical Monte Carlo simulations [30]; we performed simulations at 87.3 K for silica pores of various sizes. In Ref. 30 we focused on the relation between the modulus and pore size at saturation and did not investigate the dependence of modulus on the fluid pressure. Here we present simulation results for the elastic modulus of liquid argon at several different temperatures, both in bulk and under confinement in nanopores of different sizes and solid-fluid interaction strengths. We focus on the relation between the modulus and the Laplace pressure in the pore below the saturation, or pressure of the bulk fluid above and below the saturation pressure. We show that for all the simulated cases, the elastic modulus is a linear function of fluid pressure (in bulk) or Laplace pressure (in confinement) *with the same slope*. Moreover, we show that this slope agrees well with the slope calculated from experimental reference data for bulk liquid argon. Finally, we show that this slope is close to the slope calculated from the ultrasonic experiments of Schappert and Pelster. These comparisons demonstrate that the slope of the $K(P)$ dependence is roughly constant irrespective of the confinement. To our knowledge, this common slope has not been reported previously for confined fluids. In addition to contributing to fundamental understanding of thermodynamics of confined fluids, this common slope has useful implications for ultrasonic studies of porous materials: we discuss how our result can be applied for estimating the elastic parameters of nanoporous solids from ultrasonic experiments.

II. METHODS

A. Elastic Properties from Ultrasonic Experiments

Experimental measurements of the propagation time of ultrasonic waves give information on its velocity, which provides the information for elastic constants of materials: shear modulus G from the shear wave velocity v_s, and longitudinal modulus M from the longitudinal wave velocity v_l:

$$G = v_s^2 \rho \qquad M = v_l^2 \rho, \tag{1}$$

where ρ is the mass density of the sample. The bulk modulus of the sample can be calculated from the two measurements as [31]

$$K = M - \frac{4}{3}G. \tag{2}$$

For fluids, the shear modulus G_f is zero and therefore the longitudinal modulus is equal to the bulk modulus

$$K_f = M_f. \tag{3}$$

While the calculation of a fluid bulk modulus from ultrasonic experiments is straightforward, the calculation of the modulus of a confined fluid from the experimental ultrasonic data is non-trivial. For a given porous sample, one can measure the logitudinal and shear moduli when it is dry (M_0 and G_0) and when it is saturated, i.e., a solid-fluid composite (M_c and G_c). The differences between the corresponding moduli are determined by the properties of the fluid. Experiments for argon adsorption in Vycor glass at $T = 80$ K and $T = 86$ K show that the shear modulus of the sample does not change, $G_c \simeq G_0$ [18], which is consistent with the fact the adsorbed argon is in a liquid-like state and the shear modulus of the liquid is zero.

Experiments showed that in contrast with the constant shear modulus, the longitudinal modulus of the saturated sample M_c is several percent higher than the longitudinal modulus of the dry material M_0 [18]. Moreover, for the argon-filled pores the change of the longitudinal modulus of the sample $\Delta M = M_c - M_0$ is a function of equilibrium gas pressure p. Assuming that the properties of the solid do not change appreciably, this variation can be attributed to the change of the modulus of the confined fluid. Schappert and Pelster proposed an effective medium model to determine the longitudinal modulus of the fluid M_f from the change of the longitudinal modulus of the sample ΔM [17]

$$M_f = C\Delta M, \tag{4}$$

where the constant C is a function of parameters of the dry material (porous matrix) M_0, G_0 and pore walls (constituent solid) M_s, G_s (see Figure 1). Interestingly, Page et al. [16] used a similar proportionality relation, where the constant C was a function of different material parameters, based on works of Gassmann and Biot [32, 33]. The discussion of the constant C is beyond the scope of the current work, but it is important to note that both approaches suggest that there should be a *direct proportionality* between the measured ΔM and M_f.

Finally, taking into account $G_f = 0$ we can interpret the resulting longitudinal modulus as the bulk modulus of the fluid, i.e., $K_f = M_f$.

B. Thermodynamic Definitions of Elastic Properties

In thermodynamics the most common property that quantifies the elastic properties of a fluid is the isothermal compressibility β_T, defined as

$$\beta_T \equiv -\frac{1}{V}\left(\frac{\partial V}{\partial P}\right)_T, \tag{5}$$

where V is the volume of the fluid, P is the fluid pressure, and T is the absolute temperature. The isothermal compressibility of a bulk or confined fluid can be straightforwardly calculated from molecular simulations (See Section II C). For further consideration and for comparison with ultrasonic experiments it is convenient to discuss the reciprocal value, the isothermal elastic modulus

$$K_T = \frac{1}{\beta_T} \equiv -V\left(\frac{\partial P}{\partial V}\right)_T. \tag{6}$$

It is important to note that the modulus K_T is not the experimental bulk modulus determined from ultrasonic experiments. The experimental conditions are adiabatic rather than isothermal. Therefore the experimentally-measured bulk modulus is actually the adiabatic modulus, i.e., determined by a derivative at constant entropy S:

$$K \equiv -V\left(\frac{\partial P}{\partial V}\right)_S. \tag{7}$$

However, K and K_T are simply related through the heat capacity ratio $\gamma \equiv c_P/c_V$ [34] via

$$K_T = K/\gamma. \tag{8}$$

Ultrasonic and calorimetric measurements for bulk fluids are well-established, and thus the values of compressibilities (or moduli) for many bulk fluids are readily available for a wide range of temperatures and pressures. For argon, which is considered in this work, the reference data is given in [35–37].

Strictly speaking, in order to relate K_T and K for a confined fluid, one needs to know the heat capacity ratio γ for the *confined fluid*. However, it is unlikely that confinement has a noticeable effect on the heat capacity of argon [3, 38, 39], and moreover on the heat capacity *ratio* γ. Therefore, we use the bulk value of γ at the corresponding temperature when

converting between K_T and K for the confined fluid. Note also that confinement introduces anisotropy to the fluid, and unlike the bulk fluid it is not always sufficient to describe the pressure in terms of a scalar variable. Calculations of a pressure tensor for simple fluids in confinement show differences between the normal and tangential components [40, 41]. Our previous calculations showed that the compressibility of a confined fluid should be related to the normal component of the pressure tensor [29].

C. Calculating Elastic Properties from Molecular Simulations

Classical statistical mechanics can be used to calculate the compressibility of the fluid β_T from the fluctuations of number of particles in the pore, N, in the grand-canonical ensemble [34, 42] through the relation

$$K_T^{-1} = \beta_T = \frac{V\langle \delta N^2 \rangle}{k_{\mathrm{B}} T \langle N \rangle^2}, \tag{9}$$

where $\langle \delta N^2 \rangle = \langle N^2 \rangle - \langle N \rangle^2$ and k_{B} is Boltzmann's constant. Eq. 9 is valid when the fluctuations are normally distributed [34]. In the grand-canonical ensemble the fluid atoms or molecules in the pore are assumed to be in equilibrium with a reservoir, and the pressure p of the reservoir is the pressure of a bulk fluid at the same chemical potential and T as the fluid in the pore. Typically, the reservoir contains a gas phase whose pressure, p, differs from the pressure in the adsorbed phase, P. The schematic describing the calculation of elastic modulus from the Monte Carlo simulations is shown in Figure 2.

Here we use results from molecular simulations of argon in spherical silica pores from the grand canonical transition-matrix Monte Carlo (GC-TMMC) [43–45] method. Since this method was discussed and used in previous work [30], the reader is directed to Section II.B of Ref. 30 for a full discussion of both the simulation technique and the fluid model. In short, we modeled argon at various temperatures below its critical point both as a bulk fluid and confined in model spherical mesopores with simulation strategies identical to those in Ref. 30. The parameters used to model the argon fluid and silica material were identical to those in Ref. 30, except for simulations which varied the solid-fluid interaction strength. In the base case of argon-silica, the solid-fluid interaction parameter is $\epsilon_{\mathrm{sf}}/k_B = 171.24\ K$; to investigate the effect of varying this parameter we ran simulations at $\epsilon_{\mathrm{sf}}/k_B$ $\pm 20\%$, $\pm 50\%$ relative to the base case.

For the discussion we choose pore sizes 3.0 nm, 4.0 nm and 5.0 nm. We do not consider smaller pores, because for size smaller than ca. 2.5 nm, the number of fluid molecules in the pore become too small, the fluctuations become non-Gaussian, and Eq. 9 becomes invalid [30]. Large pores are not considered because they would require substantially higher computational cost, while not bringing new insight. By the pore sizes we refer here to the external diameter of a spherical pore d_{ext}, the distance of a line drawn through the centers of hypothetical silica solid atoms at opposite pore wall surfaces. The internal diameter is given by $d_{\text{int}} \simeq d_{\text{ext}} - 1.7168\sigma_{\text{sf}} + \sigma_{\text{ff}}$, which well approximates the accessible volume of the pore [46]. Lastly, we present results at temperatures of 77.7 K, 87.3 K, and 95.7 K; the results for confined argon at 87.3 K are taken directly from Ref. 30, the results for bulk at 87.3 K and all the results at the other temperatures are from new simulations.

III. RESULTS

GC-TMMC simulations provide the compressibility (or elastic modulus) of the fluid as a function of the relative gas pressure p/p_0, where p_0 is the saturation pressure for the fluid at the specified temperature. At $p_c < p < p_0$, where p_c is the capillary condensation pressure, a mesopore is filled with a liquid-like capillary condensate. Such system is under the action of capillary (Laplace) pressure, which causes stretching of the fluid. Note that the tension of the liquid in the mesopores is clearly seen in the X-ray diffraction patterns [47] and through the adsorption-induced deformation of the mesopores [5, 7]. The Laplace pressure can be written as a function of p/p_0 using the Kelvin-Laplace equation

$$P_L = \frac{R_g T}{V_l} \ln\left(\frac{p}{p_0}\right), \tag{10}$$

where R_g is the gas constant and V_l is the liquid molar volume. Since V_l varies only slightly with p/p_0, for simplicity we use V_l corresponding to the bulk liquid at saturation conditions in the results that follow. For $p/p_0 < 1$, P_L is necessarily negative and is indicative of the stretched nature of the fluid. Therefore, plots of the calculated modulus K_T for the confined fluid versus Laplace pressure show the variation of the fluid's elastic properties as a function of the actual pressure in the adsorbed phase. Figure 3 gives these dependences for three modeled confined systems: 3 nm, 4 nm and 5 nm pores at 87.3 K (GC-TMMC results from Ref. 30).

Similarly to our simulations results, Fig. 3 also presents the K_T moduli derived from ultrasonic experiments on argon confined in the Vycor glass nanopores from the recent works of Schappert and Pelster [18, 48] at 80 K and 86 K. We divided the adiabatic data from those papers by $\gamma = 1.969$ and $\gamma = 2.064$ for 80 K and 86 K, respectively [36]. Both series are shown as stars in Figure 3.

Figure 3 also includes the isothermal modulus K_T for bulk argon as a function of bulk fluid pressure p. The horizontal dotted line gives the K_T calculated at the saturation point $p = p_0 \simeq 0.1$ MPa at $T = 87.3$ K. This value of K_T agrees well with the experimental value $K_T = 0.47$ GPa [36]. The positively sloped line with square markers gives the simulation results for liquid bulk argon for pressures above and below the saturation pressure at 87.3 K. Below the saturation conditions, the bulk liquid is necessarily metastable and, eventually, the fluid pressure becomes negative, indicating that the fluid is stretched. Finally, three solid lines in Figure 3 show the K_T for the bulk reference data at four temperatures 85 K, 87.3 K, 90 K and 95 K (top to bottom) [36, 37].

All the data sets shown in Figure 3 (bulk and confined, theoretical and experimental) reveal one similar feature: a nearly linear dependence of K_T on pressure, either the fluid pressure for a bulk liquid or the Laplace pressure for a confined fluid. We fit the data in Figure 3 with the linear functions

$$K(P) = K_i + \alpha P. \tag{11}$$

We used all of the data points when fitting the experimental data for bulk and confined argon. When fitting the simulation data we use the data points above -10 MPa, which is the range of pressures comparable to the experimental data for confined argon. The linear fit is shown with the dashed lines of corresponding colors. The resulting fitting parameters are summarized in Table I. Except for the experimental ultrasonic data for confined argon at 86 K from [48], which is very noisy, all the other series show very close slopes of 9.0 ± 1.0.

To further examine how this linear trend depends on temperature, Figure 4 shows K_T for simulated argon in both bulk conditions and 3 and 4 nm spherical pores, at temperatures of 77.7 K, 87.3 K, and 95.7 K. Figure 4 again shows that K_T is a nearly linear function of the appropriate pressure descriptor, particularly for pressures above -10 MPa. One feature of note is a pronounced "hump" centered about -20 MPa in the 4 nm, 77.7 K data set. This feature is simply statistical noise as uncertainty in K_T is about 2% and the linear trend line

System	T (K)	α	K_i (GPa)
Bulk (exp.)	85.0	9.47	0.502
Bulk (exp.)	87.3	9.25	0.471
Bulk (exp.)	90.0	9.09	0.435
Bulk (exp.)	95.0	9.08	0.372
in Vycor (exp.)	86.0	6.47	0.568
in Vycor (exp.)	80.0	8.85	0.689
Bulk (GC-TMMC)	77.7	9.30	0.605
Bulk (GC-TMMC)	87.3	9.29	0.475
Bulk (GC-TMMC)	95.7	9.13	0.373
3 nm (GC-TMMC)	77.7	8.96	0.979
3 nm (GC-TMMC)	87.3	8.94	0.823
3 nm (GC-TMMC)	95.7	8.28	0.718
4 nm (GC-TMMC)	77.7	8.48	0.867
4 nm (GC-TMMC)	87.3	8.54	0.729
4 nm (GC-TMMC)	95.7	9.66	0.626
5 nm (GC-TMMC)	87.3	8.80	0.672

TABLE I. Slope α and intercept K_i (at $P = 0$) for the data shown in Figures 3 and 4.

falls within 2% error bars. The slopes for linear fits of the K_T data in Figure 4 are also included in Table I. Remarkably, the slope of K_T versus pressure for simulated argon falls between in the region 9.0 ± 0.7, irrespective of temperature or confinement.

Figure 5 shows the relationship between K_T and the average fluid density for simulated argon as a bulk fluid and confined in the 3, 4, and 5 nm pores, and from experimental measurements of bulk argon, all at 87.3 K. All data in the figure are for liquid or liquid-like conditions (i.e., gas-like states for the confined fluid are not included). The common trend is that K_T is a monotonically increasing function of density, and confinement increases K_T relative to the bulk fluid. We will return to this plot for specific discussion in the following section.

Figure 6 shows the effect of the solid-fluid interaction on K_T as a function of P for

spherical pores of size 3 and 4 nm, the intent of which is to show that the linear scaling trend is not specific to the argon-silica system originally studied, but extends to other materials (the interaction strength serving as a surrogate for material type). As in Figures 3 and 4, K_T is roughly linear with Laplace pressure near 0 MPa, though larger $\epsilon_{\rm sf}$ (i.e., strong solid-fluid interaction) shifts the entire trace of K_T versus P to higher values, and vice versa. The slopes of $K_T\,(P)$ for Figure 6 near $P = 0$ are shown in Table II. For all cases except the weakest interaction, that slope is again bounded by 9.0 ± 1.0, though monotonically increasing with $\epsilon_{\rm sf}$. For $\epsilon_{\rm sf}/k_B = 85.62$ K (50% reduction relative to the base argon-silica case), the slopes are close to 7.0. Additionally, there is an inversion in the modulus as a function of the solid-fluid interaction; for this case, the K_T for the 4 nm pore is larger than that for 3 nm where the opposite is true for the other values of $\epsilon_{\rm sf}$. We note for this case that the solid-fluid interaction is weaker than the fluid-fluid interaction ($\epsilon_{\rm ff}/k_B = 119.6$ K [30]), so the confinement is effectively solvophobic[49].

System	$\epsilon_{\rm sf}/k_B$ (K)	α
3 nm	85.62	6.80
3 nm	136.99	8.09
3 nm	171.24	8.94
3 nm	205.49	9.47
3 nm	256.86	9.72
4 nm	85.62	7.19
4 nm	136.99	8.17
4 nm	171.24	8.54
4 nm	205.49	9.49
4 nm	256.86	9.78

TABLE II. Slope α (at $P = 0$) calculated from GC-TMMC data as a function of solid-fluid interaction strength for 3 nm and 4 nm pores, based on the data shown in Figure 6.

IV. DISCUSSION

The linear relation between K_T of a bulk fluid or a bulk solid and the applied pressure (Eq. 11) has been known for decades. It is often referred to as the "modified Tait equation" [50] or Tait-Murnaghan equation, originating from the seminal work of Murnaghan [51]. Eq. 11 is obviously a linearization of the $K(P)$ dependence. However, the range in which linearization works is very wide: for organic liquids it works well up to pressures ca. 100 MPa and for water up to ca. 1 GPa [52].

For bulk liquids the slope α in the $K(P)$ relation has been also discussed. Wilhelm pointed out that for a number of organic liquids this slope is practically independent of the temperature, and almost independent of the fluid, always about $\alpha \simeq 9 - 10$ [53]. Wilhelm also proposed an analytic expression for the slope α based on the Carnahan-Starling equation of state [54] with a cohesive term [53]. His calculations were in good agreement with the experimental data for hydrocarbons. Using Wilhelm's theory we calculated the slope α for argon, using 3.48 Å as a hard sphere diameter [55] and the reference data for the triple point from [36], yielding $\alpha = 8.2$, which is fairly close to the values of α calculated directly from reference data (Table I). We have to note that α is not a universal constant: its value for water (ca. 5.8 [53]) and most solids [56] is significantly lower.

Although one of us [29] had previously pointed out that K_T has a linear dependence on pressure and the slopes agreed well with the experimental data from Ref. 18, we did not compare the confined fluid results to those of a bulk fluid. In the present work, we aggregate the results of simulations and experiments for both bulk and confined argon at multiple temperatures, and are thus able to conclude that, irrespective of whether the fluid is bulk or confined, its isothermal elastic modulus approximately satisfies a linear $K(P)$ relation (Tait-Murnaghan equation) with slope α that is only weakly dependent on either temperature or the nature of confinement. Therefore, our results show that nanoconfinement, while strongly affecting K_T of the fluid (essentially, making the fluid stiffer), does not affect its pressure derivative dK_T/dP, the parameter α in the linear relation Eq. 11. We note that it is not the confinement *per se* that increases K_T; the modulus is increased due to strong solid-fluid attraction forces. In the case of solid-fluid interactions that are weaker than fluid-fluid interaction (e.g. water in hydrophobic confinement), the opposite effect is observed: the value of K_T in confinement is lower than the modulus of the bulk fluid [57–60].

As a general rule, higher density makes a fluid stiffer, i.e., increases the modulus K_T. That is indeed true for each of the data series in this work considered independently. However, the data in Figure 5 clearly show that although the confined fluid has lower density than liquid argon (near saturation) at 87.3 K, it has a higher modulus. Therefore, increased average density is not sufficient to explain the increase in K_T for a confined fluid. Specifically, we note in Figure 5 that the 3 nm pore has generally lower average density than the other pores, yet has the highest modulus. It is likely that the reason for higher modulus of the confined fluid is due to contribution of the first 1-2 layers of fluid next to the pore wall. These layers are known to be solid-like [61], therefore the "local" modulus for these layers should be much higher than for molecules near the pore center. Experimental data for K_T of solid argon at 77 K is ca. 1.4 GPa [62–64], i.e., larger than K_T for liquid argon by a factor of three. For smaller pores, the contribution of these solid-like layers to the overall modulus is higher and therefore the modulus of fluids in small pores significantly exceeds the bulk liquid value [30]. Unlike the modulus itself, the slope α of $K(P)$ dependence for solid argon is very close to that of the liquid, $\alpha = 9.95$ [64]. This small difference explains our observation for confined fluids: while the modulus is noticeably higher for a given average density (due to the contribution of surface layers), the slope α is the same, because the solid-like layers still have the same α.

The simulation results in Figure 6 test whether this common α extends to other materials for a given fluid. That figure clearly indicates that a linear trend near $P = 0$ is preserved regardless of solid-fluid interaction strength and the α parameters in Table II fall in the same bounds (9.0 ± 1.0) provided that the confinement is solvophilic ($\epsilon_{\mathrm{sf}} > \epsilon_{\mathrm{ff}}$). This further suggests that the α parameter can be treated as a thermodynamic property of the fluid, not of the confining material, confinement dimensions, or temperature. Table II also shows another new trend, that α appears to increase monotonically with solid-fluid strength, and prompts the question of whether further increasing ϵ_{sf} would take α outside the range of 9.0 ± 1.0. We do not expect a further increased ϵ_{sf} to alter α outside this range as packing constraints on the fluid near the material surface will prevent excessive densification of the confined fluid. Conversely, the weakening of ϵ_{sf} to solvophobic conditions does lead to α outside the range of the bulk fluid. This is, however, expected due to the altered physics of the solvophobic confinement, in which the confined fluid is rarefied near the surface (compared to solvophilic confinement) and behaves more like a coalesced liquid than a typical capillary-confined

fluid[57, 58, 65–68].

Our findings for the α of confined fluids further extend the broad commonality of this thermodynamic parameter, widely discussed in the past for the bulk fluids [53]. In addition to the fundamental interest, this result imposes an important constraint on the analysis of ultrasonic data for fluid-saturated porous materials. Effective medium approaches, be it the one proposed by Schappert and Pelster [17], or the one based on Biot-Gassmann equations [32, 33], suggest that there is a direct proportionality between the change of the measured longitudinal modulus of the porous sample ΔM and modulus of the fluid M_f (e.g., Eq. 4). The proportionality coefficient C in this relation depends on the elastic properties of the dry porous sample, and the properties of the solid walls. While the former can be easily measured, the latter are hard to measure directly, and indirect methods for estimating them may be non-trivial and involve certain assumptions about the microstructure [30, 69]. However, the general result of this work, i.e., the common slope α of the $K(P)$ line, imposes a constraint on Eq. 4, and unambiguously determines the value of the constant C in this relation. Therefore, one can readily compare the slope of the experimentally measured dependence of $\Delta M = \Delta M(p/p_0) = \Delta M(P_L)$ to the slope α of the reference K_T data for the same fluid and to calculate the translation coefficient C from this comparison. Analysis of the value of C based on an effective medium approach will then provide the information of the elastic constant of the pore walls (solid constituent).

V. CONCLUSION

We have studied the elastic modulus-pressure dependence $K(P)$ for confined and bulk liquid argon. For bulk fluids and solids this dependence is well described by a linear function $K(P) = K(0) + \alpha P$, known as Tait-Murnaghan equation. We have used transition-matrix Monte Carlo simulations to calculate the isothermal elastic modulus K_T of argon in bulk and confined in silica mesopores. Our calculations have shown that although K_T is strongly affected by confinement, its dependence on pressure can still be described by the linear Tait-Murnaghan equation. The calculated slope α for confined argon is the same as α calculated for bulk one provided that the confinement is not solvophobic; moreover, it agrees well with the reference data for bulk argon and experimental data for confined argon derived from ultrasonic experiments. Also it does not appreciably changes with temperature. In addition

to shedding more light on thermodynamics of confined fluids, our results advance the analysis of ultrasonic experiments on fluid-saturated porous samples. Knowledge of the slope α of the $K(P)$ dependence can be applied as a constraint to the analysis of experimental ultrasonic data, making it possible to estimate the elastic properties of an unknown porous medium.

ACKNOWLEDGMENT

This research was performed while one of the authors (G.G.) held a National Research Council Research Associateship Award at Naval Research Laboratory. The work of G.G. and N.B. was funded by the Office of Naval Research through the Naval Research Laboratory's basic research core program. G.G. thanks Rolf Pelster and Klaus Schappert for the fruitful discussions of ultrasonic data, George Scherer for discussion of mechanical properties of Vycor glass, and Patrick Huber for the argon heat capacity data.

---

[1] P. Huber, J. Phys.: Condens. Matter **27**, 103102 (2015).

[2] K. Morishige and K. Kawano, J. Chem. Phys. **110**, 4867 (1999).

[3] D. Wallacher and K. Knorr, Phys. Rev. B **63**, 104202 (2001).

[4] K. Morishige and K. Mikawa, J. Phys. Chem. C **116**, 14979 (2012).

[5] G. Günther, J. Prass, O. Paris, and M. Schoen, Phys. Rev. Lett. **101**, 086104 (2008).

[6] Y. Long, J. C. Palmer, B. Coasne, M. Śliwinska-Bartkowiak, and K. E. Gubbins, Microporous Mesoporous Mater. **154**, 19 (2012).

[7] G. Y. Gor, O. Paris, J. Prass, P. A. Russo, M. M. L. Ribeiro Carrott, and A. V. Neimark, Langmuir **29**, 8601 (2013).

[8] D. Morineau and C. Alba-Simionesco, J. Chem. Phys. **118**, 9389 (2003).

[9] Y. B. Melnichenko, *Small-angle Scattering from Confined and Interfacial Fluids: Applications to Energy Storage and Environmental Science* (Springer, 2015).

[10] W. F. Murphy III, J. Acoust. Soc. Am. **71**, 1458 (1982).

[11] J. R. Beamish, A. Hikata, L. Tell, and C. Elbaum, Phys. Rev. Lett. **50**, 425 (1983).

[12] J. Beamish, A. Hikata, and C. Elbaum, Phys. Rev. Lett. **52**, 1790 (1984).

[13] N. Mulders and J. R. Beamish, Phys. Rev. Lett. **62**, 438 (1989).

[14] K. L. Warner and J. R. Beamish, J. Appl. Phys. **63**, 4372 (1988).

[15] J. H. Page, J. Liu, B. Abeles, H. W. Deckman, and D. A. Weitz, Phys. Rev. Lett. **71**, 1216 (1993).

[16] J. H. Page, J. Liu, B. Abeles, E. Herbolzheimer, H. W. Deckman, and D. A. Weitz, Phys. Rev. E **52**, 2763 (1995).

[17] K. Schappert and R. Pelster, J. Phys.: Condens. Matter **25**, 415302 (2013).

[18] K. Schappert and R. Pelster, EPL **105**, 56001 (2014).

[19] E. Molz, A. P. Y. Wong, M. H. W. Chan, and J. R. Beamish, Phys. Rev. B **48**, 5741 (1993).

[20] E. B. Molz and J. R. Beamish, J. Low Temp. Phys. **101**, 1055 (1995).

[21] G. Beaudoin, P. Haljan, M. Paetkau, and J. R. Beamish, J. Low Temp. Phys. **105**, 113 (1996).

[22] E. V. Charnaya, P. G. Plotnikov, D. Michel, C. Tien, B. F. Borisov, I. G. Sorina, and E. I. Martynova, Physica B: Condensed Matter **299**, 56 (2001).

[23] B. F. Borisov, A. V. Gartvik, F. V. Nikulin, and E. V. Charnaya, Acoustical physics **52**, 138 (2006).

[24] K. Schappert and R. Pelster, Phys. Rev. B **78**, 174108 (2008).

[25] E. V. Charnaya, Acoustical Physics **54**, 802 (2008).

[26] B. F. Borisov, A. V. Gartvik, A. G. Gorchakov, and E. V. Charnaya, Phys. Solid State **51**, 823 (2009).

[27] K. Schappert and R. Pelster, Phys. Rev. B **83**, 184110 (2011).

[28] K. Schappert and R. Pelster, Phys. Rev. Lett. **110**, 135701 (2013).

[29] G. Y. Gor, Langmuir **30**, 13564 (2014).

[30] G. Y. Gor, D. W. Siderius, C. J. Rasmussen, W. P. Krekelberg, V. K. Shen, and N. Bernstein, J. Chem. Phys. **143**, 194506 (2015).

[31] R. E. Goodman, *Introduction to rock mechanics*, vol. 2 (Wiley New York, 1989).

[32] F. Gassmann, Viertel. Naturforsch. Ges. Zürich **96**, 1 (1951).

[33] M. A. Biot, J. Acoust. Soc. Am. **28**, 168 (1956).

[34] L. D. Landau and E. M. Lifshitz, *Statistical Physics, vol. 5*, vol. 30 (Pergamon, 1980).

[35] R. B. Stewart and R. T. Jacobsen, J. Phys. Chem. Ref. Data **18**, 639 (1989).

[36] C. Tegeler, R. Span, and W. Wagner, J. Phys. Chem. Ref. Data **28**, 779 (1999).

[37] E. W. Lemmon, M. O. McLinden, and D. G. Friend, in *NIST Chemistry WebBook,NIST Standard Reference Database 69*, edited by P. J. Linstrom and W. G. Mallard

(http://webbook.nist.gov, retrieved June 13, 2016).

[38] P. Huber and K. Knorr, Phys. Rev. B **60**, 12657 (1999).

[39] K. Knorr, D. Wallacher, P. Huber, V. Soprunyuk, and R. Ackermann, Eur. Phys. J. E Soft Matter **12**, 51 (2003).

[40] E. N. Brodskaya, A. I. Rusanov, and F. M. Kuni, Colloid J. **72**, 602 (2010).

[41] Y. Long, M. Śliwińska-Bartkowiak, H. Drozdowski, M. Kempiński, K. A. Phillips, J. C. Palmer, and K. E. Gubbins, Colloids Surf., A **437**, 33 (2013).

[42] M. Allen and D. Tildesley, *Computer simulation of liquids. 1987*, vol. 385 (New York: Oxford, 1989).

[43] J. R. Errington, J. Chem. Phys. **118**, 9915 (2003).

[44] V. K. Shen and J. R. Errington, J. Phys. Chem. B **108**, 19595 (2004).

[45] D. W. Siderius and V. K. Shen, J. Phys. Chem. C **117**, 5861 (2013).

[46] G. Y. Gor, C. J. Rasmussen, and A. V. Neimark, Langmuir **28**, 12100 (2012).

[47] K. Morishige and H. Yasunaga, J. Phys. Chem. B **110**, 3864 (2006).

[48] K. Schappert and R. Pelster, Langmuir **30**, 14004 (2014).

[49] L. D. Gelb, K. E. Gubbins, R. Radhakrishnan, and M. Sliwinska-Bartkowiak, Rep. Prog. Phys. **62**, 1573 (1999).

[50] J. R. Macdonald, Reviews of Modern Physics **38**, 669 (1966).

[51] F. D. Murnaghan, Proc. Natl. Acad. Sci. U.S.A. **30**, 244 (1944).

[52] A. T. J. Hayward, Br. J. Appl. Phys. **18**, 965 (1967).

[53] E. Wilhelm, J. Chem. Phys. **63**, 3379 (1975).

[54] N. F. Carnahan and K. E. Starling, J. Chem. Phys. **51**, 635 (1969).

[55] E. Wilhelm, J. Chem. Phys. **60**, 3896 (1974).

[56] O. L. Anderson, J. Phys. Chem. Solids **27**, 547 (1966).

[57] E. G. Strekalova, M. G. Mazza, H. E. Stanley, and G. Franzese, Phys. Rev. Lett. **106**, 145701 (2011).

[58] R. Evans and M. C. Stewart, J. Phys.: Condens. Matter **27**, 194111 (2015).

[59] R. Evans and N. B. Wilding, Phys. Rev. Lett. **115**, 016103 (2015).

[60] K. Nygård, S. Sarman, K. Hyltegren, S. Chodankar, E. Perret, J. Buitenhuis, J. F. van der Veen, and R. Kjellander, Physical Review X **6**, 011014 (2016).

[61] S. Granick, Science **253**, 1374 (1991).

[62] J. W. Stewart, J. Phys. Chem. Solids **29**, 641 (1968).

[63] M. S. Anderson and C. A. Swenson, J. Phys. Chem. Solids **36**, 145 (1975).

[64] A. N. Utyuzh and V. V. Kechin, Sov. Phys. JETP **58**, 460 (1983).

[65] A. Striolo, K. E. Gubbins, A. A. Chialvo, and P. T. Cummings, Mol. Phys. **102**, 243 (2004).

[66] T. Kimura, H. Kanoh, T. Kanda, T. Ohkubo, Y. Hattori, Y. Higaonna, R. Denoyel, and K. Kaneko, J. Phys. Chem. **108**, 14043 (2004).

[67] J. C. Liu and P. A. Monson, Langmuir **21**, 10219 (2005).

[68] E. G. Strekalova, M. G. Mazza, H. E. Stanley, and G. Franzese, J. Phys.: Condens. Matter **24**, 064111 (2012).

[69] G. W. Scherer, J. Am. Ceram. Soc. **69**, 473 (1986).

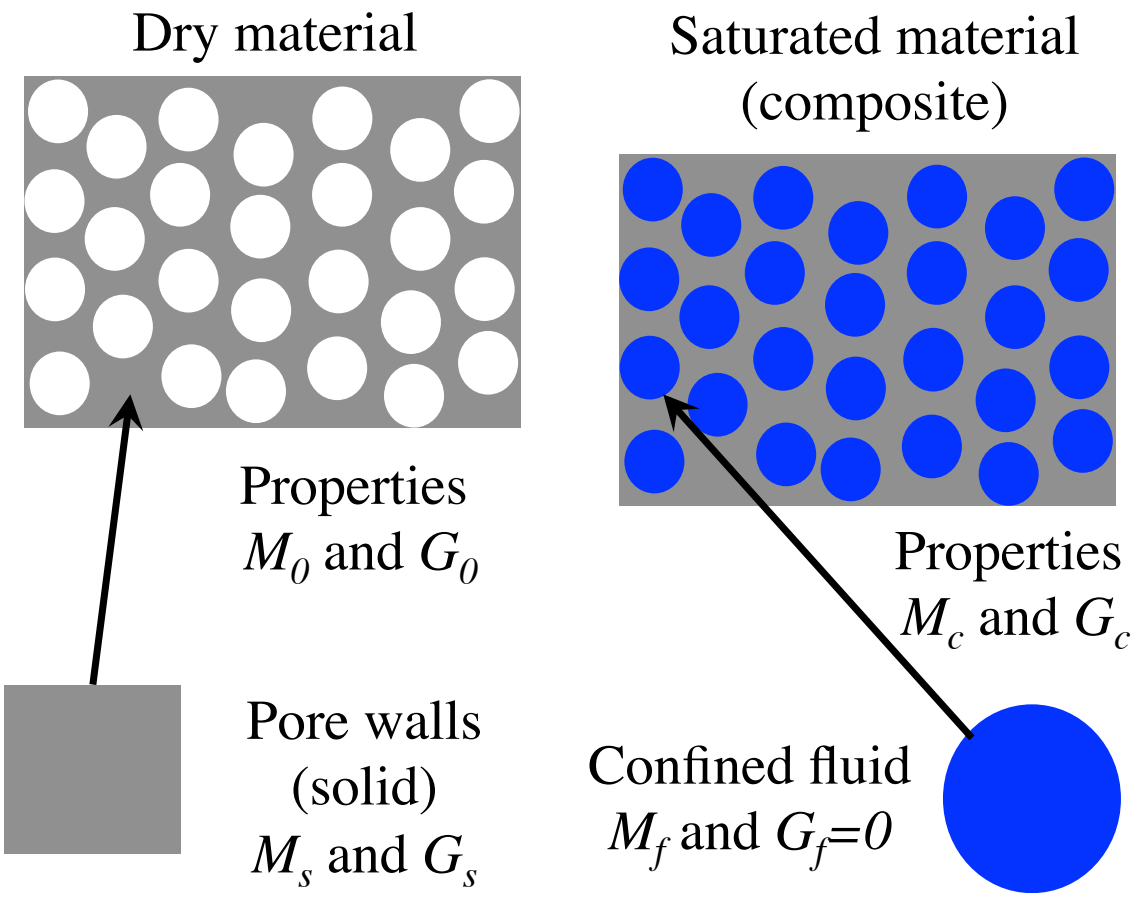

FIG. 1. Schematic of a fluid-saturated porous material as a composite, with denotations for various elastic moduli.

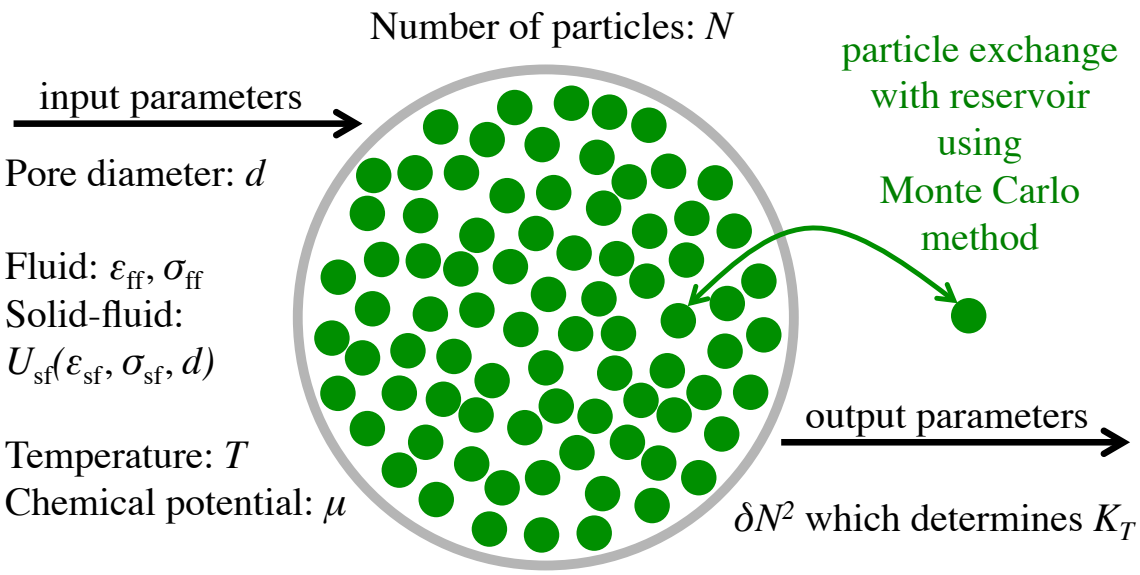

FIG. 2. Schematic of calculation of elastic modulus of confined fluid from Monte Carlo simulations in grand canonical ensemble. Required input parameters are the pore size d, LJ parameters for fluid particles ϵ_{ff} and σ_{ff}, LJ parameters for solid-fluid interactions ϵ_{sf} and σ_{sf}, temperature T and chemical potential of the fluid μ. The resulting elastic modulus is calculated from the fluctuation of number of particles in the system using Eq. 9.

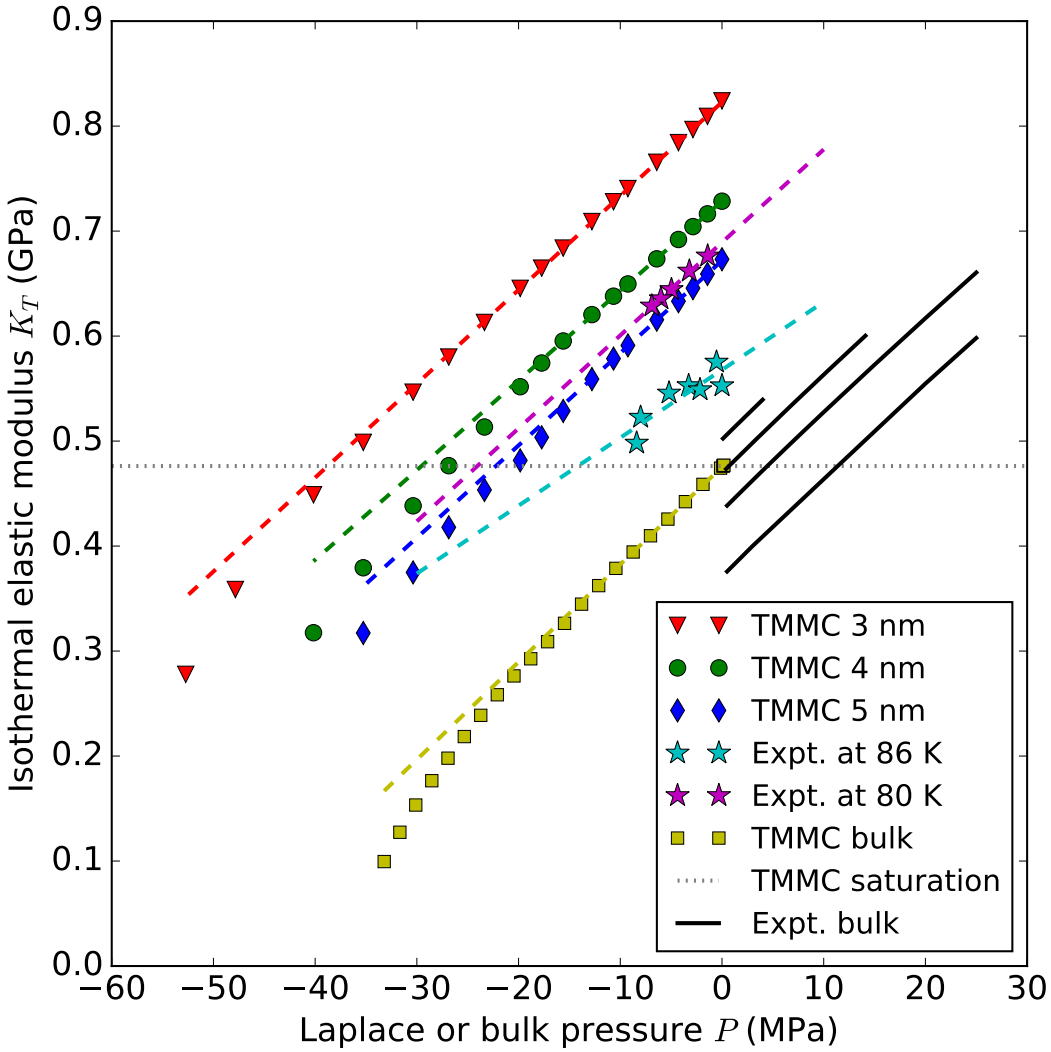

FIG. 3. Liquid argon isothermal elastic modulus K_T as a function of pressure p or Laplace pressure P_L for bulk and confined systems, respectively. Black solid lines show the experimental reference data for bulk argon at temperatures of 85 K, 87.3 K, 90 K and 95 K (top to bottom), from Ref. 36. The stars are the moduli calculated based on the ultrasonic experiments for confined argon from Refs. 18 and 48, other symbols are the results of GC-TMMC calculations, and dashed lines show the linear fit for each series. The horizontal dotted line indicates K_T of bulk argon at saturation point at 87.3 K calculated by GC-TMMC.

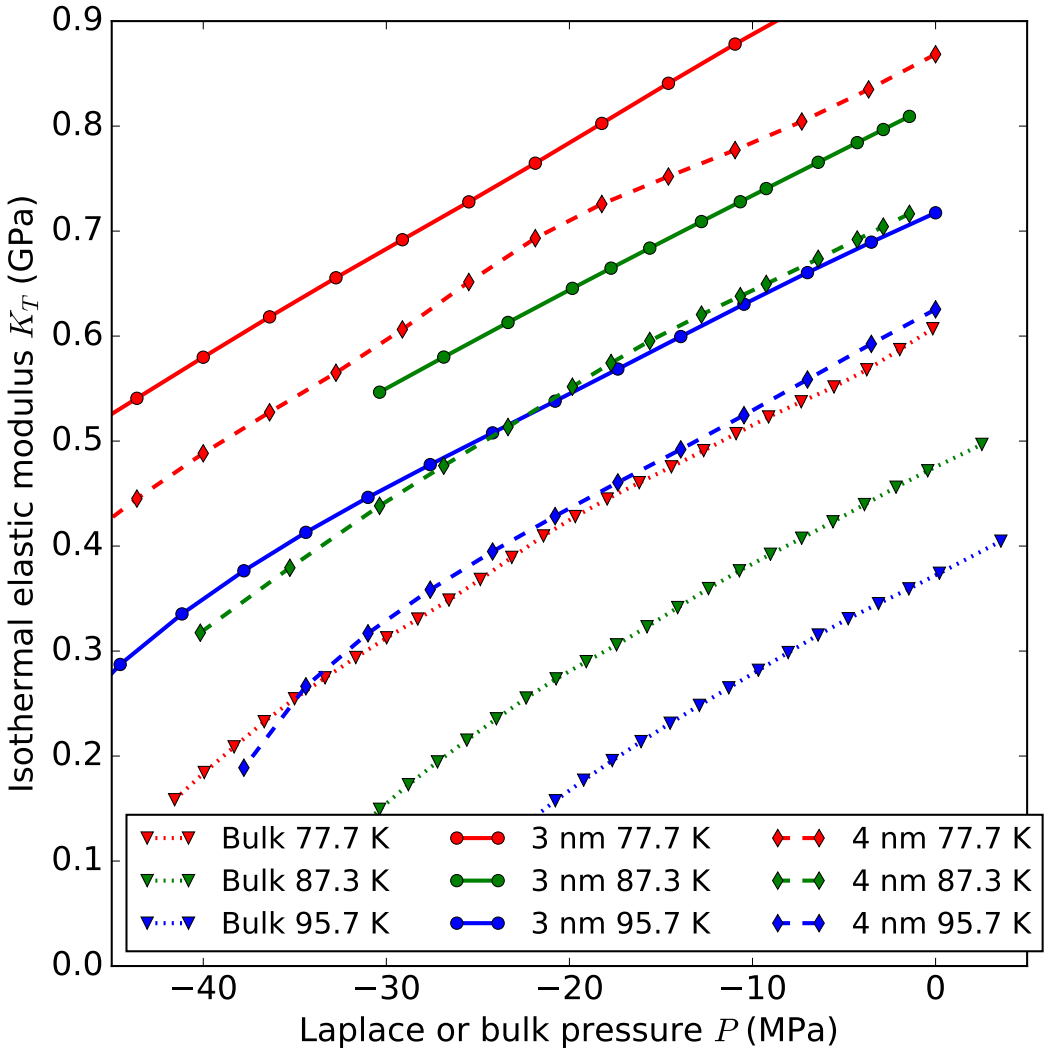

FIG. 4. Simulation results for the isothermal elastic modulus of liquid argon K_T as a function of pressure p for bulk system the pressure, and as a function of Laplace pressure P_L for confined systems with noted pore sizes, at temperatures of 77.7 K, 87.3 K, and 95.7 K.

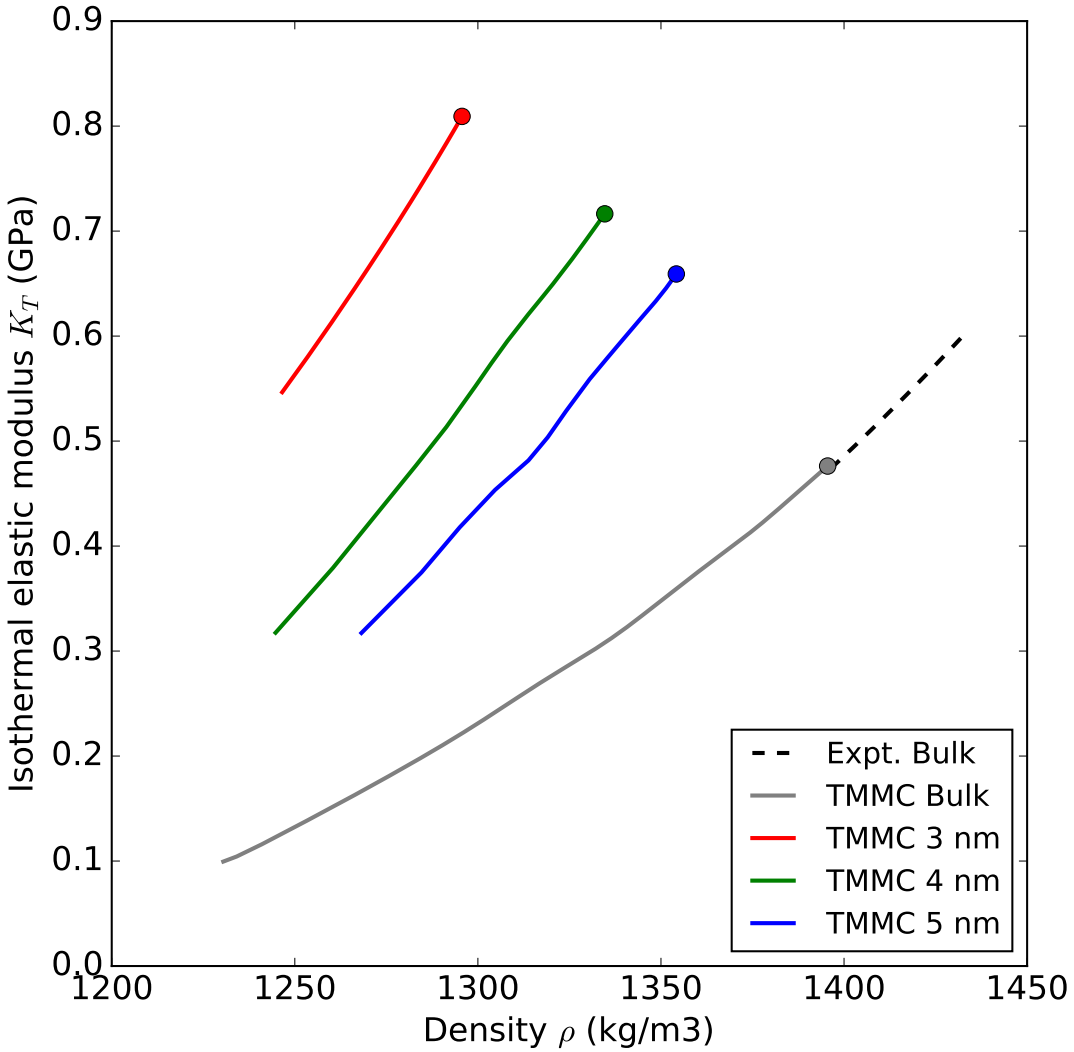

FIG. 5. Isothermal elastic modulus of liquid argon K_T at 87.3 K as a function of density in bulk (experimental data and simulations) and confined fluid (simulations). The markers correspond to the saturation points.

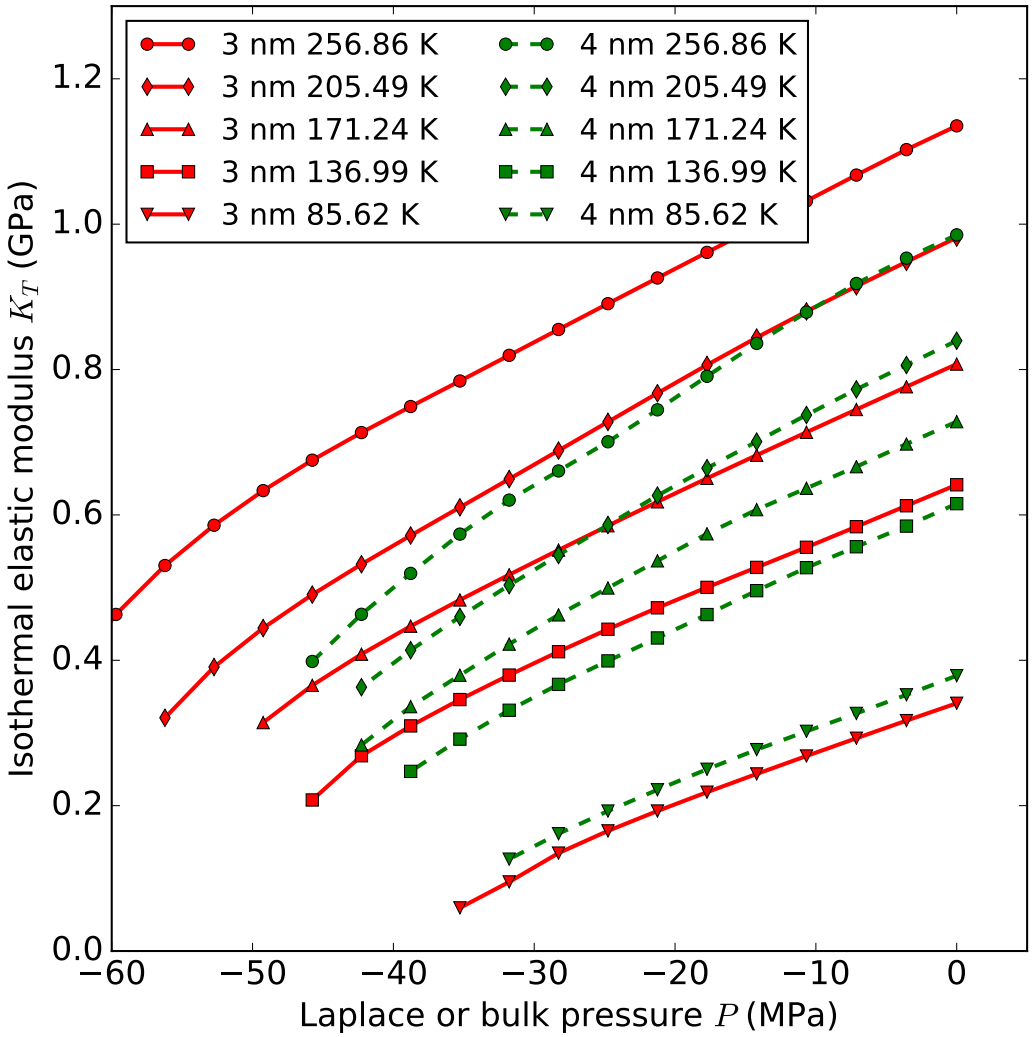

FIG. 6. Isothermal elastic modulus of liquid argon K_T at 87.3 K as a function of Laplace pressure P, with varying solid-fluid interaction strength. Solid lines (red) are for external diameter 3 nm and dash lines (green) are for 4 nm. Solid-fluid interaction parameter $\epsilon_{\rm sf}/k_B$, is altered −50%, −20%, 0%, +20%, and +50% relative to the original value of 171.24 K. The values of $\epsilon_{\rm sf}/k_B$ for each of the lines are given in the legend.